De novo purine metabolism is a metabolic vulnerability of cancers with low p16 expression

Naveen Kumar Tangudu[1,2#], Raquel Buj[1,2#], Jiefei Wang[2,3], Aidan R. Cole[1,2], Apoorva Uboveja[1,2], Richard Fang[1,2], Amandine Amalric[1,2], Maureen A. Lyons[2], Uma R. Chandran[2,3], and Katherine M. Aird[1,2*]

[1] Department of Pharmacology & Chemical Biology, University of Pittsburgh School of Medicine, Pittsburgh, PA

[2] UPMC Hillman Cancer Center, Pittsburgh, PA

[3] Department of Biomedical Informatics, University of Pittsburgh School of Medicine, Pittsburgh, PA

[#]Co-first authors

* Corresponding Author
Katherine M. Aird, PhD
Associate Professor
5051 Centre Ave.
Office: 2041; Lab: 2050
Pittsburgh, PA 15213
412-648-4823
katherine.aird@pitt.edu

Running title: Nucleotide metabolism is a vulnerability of p16-low cancer

Keywords: melanoma, one carbon metabolism, folate metabolism, anti-metabolites, anti-folates

Abstract

p16 is a tumor suppressor encoded by the *CDKN2A* gene whose expression is lost in ~50% of all human cancers. In its canonical role, p16 inhibits the G1-S phase cell cycle progression through suppression of cyclin dependent kinases. Interestingly, p16 also has roles in metabolic reprogramming, and we previously published that loss of p16 promotes nucleotide synthesis via the pentose phosphate pathway. Whether other nucleotide metabolic genes and pathways are affected by p16/*CDKN2A* loss and if these can be specifically targeted in p16-low tumors has not been previously explored. Using CRISPR KO libraries in multiple isogenic melanoma cell lines with wildtype p16/*CDKN2A* and p16/*CDKN2A* knockdown, we determined that many nucleotide metabolism genes are negatively enriched in p16/*CDKN2A* knockdown cells compared to controls. Indeed, many of the genes that are required for survival in the context of low p16/*CDKN2A* expression based on our CRISPR screens are upregulated in p16/*CDKN2A* knockdown melanoma cells and those with endogenously low *CDKN2A* expression**.** We determined that cells with low p16 expression are sensitive to multiple inhibitors of *de novo* purine synthesis *in vitro* by inducing apoptosis. Together, our data provide evidence to reevaluate the utility of these drugs in patients with p16-low tumors as loss of p16 may provide a therapeutic window for these agents.

Introduction

p16, encoded by the *CDKN2A* locus, is a critical cell cycle regulator that inhibits CDK4/6 (Sherr, 2001). Given its importance in the cell cycle, p16 is a well-known tumor suppressor with ~50% of all human tumors showing decreased expression or activity of p16 through a variety of mechanisms, including hypermethylation or deletion of the *CDKN2A* locus or mutations (Esteller et al., 2001; Inoue and Fry, 2018; Ruas et al., 1999). In melanoma, ~30% of patients have a deep deletion of the *CDKN2A* locus and another 10-15% have mutations in p16 (Zhao et al., 2016). In spite of this, there are currently no FDA-approved therapies that are used specifically for these patients, although clinical trials of CDK4/6 inhibitors are ongoing in combination both mutant BRAF inhibitors and immune checkpoint blockade (Garutti et al., 2021; Lelliott et al., 2022) (clinicaltrials.gov).

We and others have published that p16 has roles beyond cell cycle control, and some of these non-canonical roles are related to metabolism (Buj and Aird, 2019). We published in the context of senescence that loss of p16 expression promotes nucleotide synthesis at least in part via increased translation of the pentose phosphate pathway (PPP) enzyme ribose-5-phosphate isomerase A (RPIA) (Buj et al., 2019). However, glucose tracing through the PPP indicated that additional pathways may contribute to the increase in steady state nucleotide levels observed in these cells. Moreover, there is currently no available RPIA inhibitor. Therefore, the goal of this study was to identify additional nucleotide metabolism pathways that are specifically vulnerable to inhibition in p16-low cancers using melanoma as a model.

Nucleotide homeostasis is critical for cellular fidelity as nucleotides are not only used for energy and biomass, but also as signaling molecules and to cope with DNA damage (Aird and Zhang, 2015; Ali and Ben-Sahra, 2023; Shi et al., 2023; Turgeon et al., 2018). As such, multiple metabolic

pathways feed into *de novo* nucleotide synthesis, and nucleotides can also be salvaged through catabolism or the microenvironment (Buj and Aird, 2018; Kohnken et al., 2015; Lane and Fan, 2015; Tong et al., 2009). Glucose via the PPP is used to synthesize PRPP, the pentose sugar backbone of all nucleotides. One carbon metabolism is also critical, especially for *de novo* purine synthesis as purine carbons are derived from serine via the folate cycle (Yang and Vousden, 2016). Other metabolites that contribute to *de novo* synthesis include aspartate, glycine, and glutamine, thereby connecting a variety of metabolic pathways with nucleotide biosynthesis (Tong et al., 2009). It is well-known that many of these pathways are highly upregulated in cancer cells. Indeed, anti-folates and anti-metabolites were some of the first used chemotherapies, and many are still used today. Whether these drugs could benefit patients with p16-low tumors has not been investigated.

Using CRISPR KO libraries in isogenic p16 wildtype and shp16 cells, in addition to dependency scores from DepMap, we identified 31 common nucleotide metabolism genes that are negatively enriched in p16/*CDKN2A*-low cells. Many of these are either transcriptionally or translationally upregulated. Therapeutic targeting of pathways that promote *de novo* purine synthesis, including one carbon metabolism, demonstrated that p16-low cells are specifically vulnerable to inhibition of these pathways *in vitro*. Our data suggest p16 loss may create a therapeutic window to kill cancer cells.

Results

CRISPR dropout screens identify multiple nucleotide metabolism vulnerabilities in shp16/shCdkn2a cells

We previously published that knockdown of p16 increases nucleotide synthesis via translation of the PPP enzyme RPIA (Buj et al., 2019). There are no available RPIA inhibitors; thus, we set out

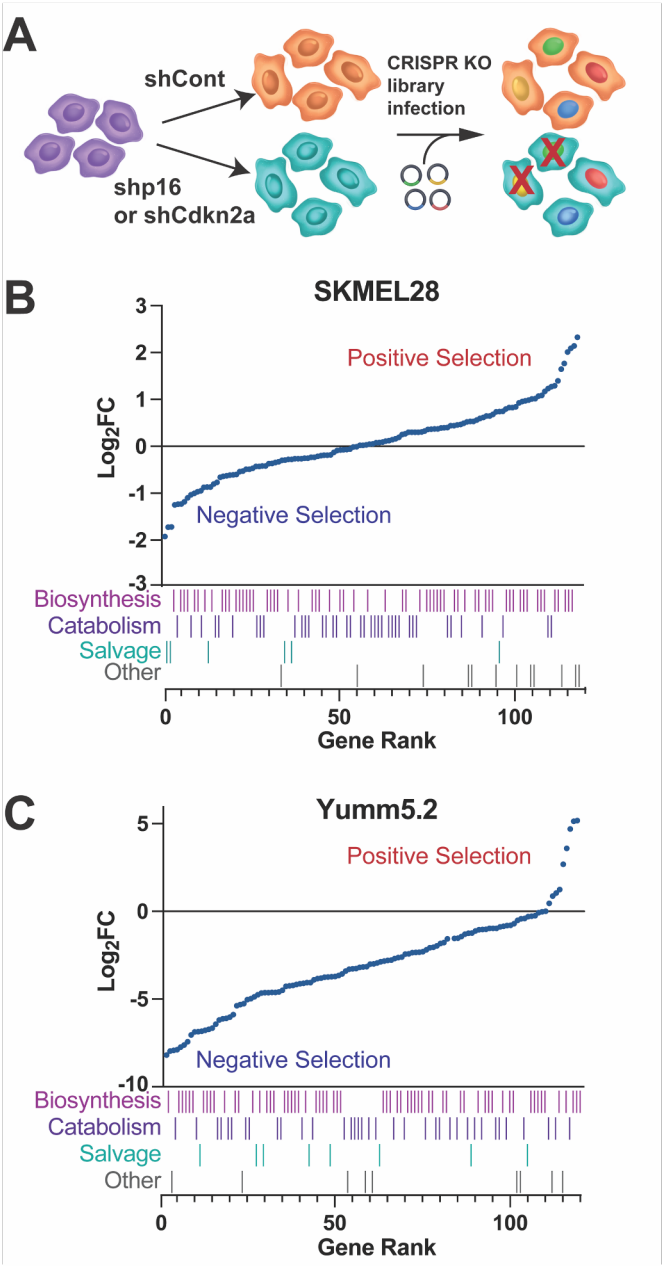

Figure 1. Multiple CRISPR knockout screens identify nucleotide metabolism genes that are selectively depleted in shp16/sh*Cdkn2a* cells. (A) Schematic of our CRISPR screens. Isogenic p16/*Cdkn2a* wildtype cells were infected with lentiviruses expression shGFP control (shCont) or shp16 (human) or sh*Cdkn2a* (mouse). These cells were infected with the CRISPR gRNA libraries at an MOI of 0.2-0.3. After 14 days in culture, gDNA was harvested and sequenced. **(B-C)** Analysis of 128 genes related to nucleotide synthesis, salvage, and catabolism identified multiple genes that are negatively selected in shp16/shCdkn2a vs. shControl in human SKMEL28 **(B)** and mouse Yumm5.2 **(C)** melanoma cells.

to identify additional nucleotide metabolic enzymes that are vulnerabilities of shp16 cells. We constructed a focused sgRNA library of 128 genes involved in nucleotide biosynthesis, salvage, and catabolism (**Table S1**) and performed a loss-of-function screen in SKMEL28 melanoma cells with wildtype p16 and p16 knockdown (**Fig. 1A and S1A**) using a hairpin that we have previously characterized that can be rescued by p16 overexpression (Buj et al., 2019). As expected, these cells proliferate faster than isogenic controls (**Fig. S1B**). Using MAGeCK analysis (Li et al., 2014), we observed negative selection for many genes involved in nucleotide homeostasis (**Fig. 1B and Table S2**). This included *RPIA*, demonstrating the validity of our screen (**Fig. S1C**). We next performed a secondary drop out screen in a mouse melanoma cell line, Yumm5.2, using a library focused on all metabolic genes (Zhu et al., 2021) and analyzed nucleotide biosynthesis and salvage genes. In Yumm5.2 cells, using a different hairpin targeting *Cdkn2a*, the gene encoding p16 (**Fig. S1D**), almost all nucleotide metabolism genes dropped out (**Fig. 1C and Table S3**). Data taken from Dependency Map (DepMap) using cutaneous melanoma cell lines also indicated increased dependency on several nucleotide metabolism genes based on *CDKN2A* expression (**Fig. S1E**). Together, these screens identified 31 common genes, many that were related to *de novo* purine synthesis and one carbon metabolism (**Table S4**). These data suggest multiple nucleotide metabolism pathways are a vulnerability in cells with low p16/*CDKN2A* expression.

p16/*CDKN2A* expression negatively correlates with nucleotide metabolism gene expression, polysome enrichment, and protein expression

Next, we cross-compared these 128 nucleotide metabolism genes to RNA-Seq data and found that multiple genes were both depleted in the CRISPR screen and transcriptionally upregulated in shp16 cells (**Fig. 2A and Table S5**). As we previously published that the PPP enzyme *RPIA* is translationally regulated (Buj et al., 2019), we also performed polysome fractionation followed by RNA-Seq (Poly-Seq). This analysis identified additional nucleotide metabolism transcripts that are

also both depleted in the CRISPR screen and translationally upregulated in shp16 cells (**Fig. 2B and Table S6**). Of the 31 common genes, 23 (~75%) are either transcriptionally or translationally upregulated in shp16 cells and many correspond to either *de novo* purine synthesis or one carbon metabolism (**Fig. 2C**). Using data from the DepMap, we found many of these 23 genes and proteins correlate with *CDKN2A* mRNA in cutaneous melanoma cell lines (**Fig. 2D-E**). Together, these data demonstrate upregulation of multiple nucleotide metabolism enzymes in the context of p16 loss.

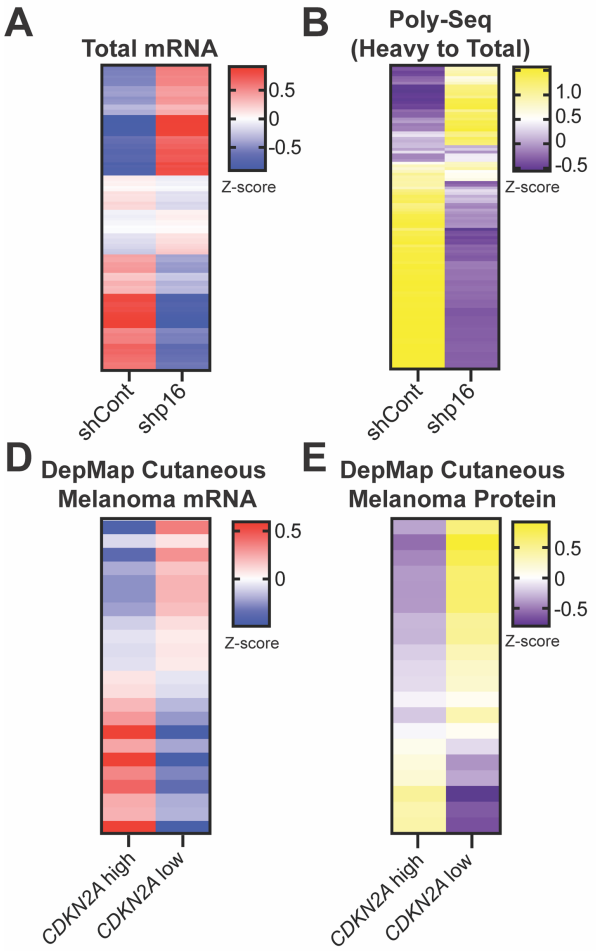

C

Genes Transcriptionally or Translationally Upregulated in shp16 vs. shCont

Gene	Pathway
ADSL	De Novo Purine biosynthesis
AK1	De Novo Purine biosynthesis
GART	De Novo Purine biosynthesis
IMPDH1	De Novo Purine biosynthesis
MTAP	De Novo Purine biosynthesis
CTPS2	De Novo Pyrimidine biosynthesis
DHFR	Folate metabolism
MTHFD1L	Folate metabolism
AMT	Glycine metabolism
GCSH	Glycine metabolism
GNMT	Glycine metabolism
GOT2	Nucleotide biosynthesis
ENTPD8	Nucleotide catabolism
NT5C2	Nucleotide catabolism
PAPSS1	Nucleotide catabolism
RPIA	Pentose phosphate pathway
CANT1	Purine catabolism
ENPP4	Purine salvage
ITPA	Purine salvage
DPYD	Pyrimidine salvage
UCK1	Pyrimidine salvage
PSAT1	Serine metabolism
UCKL1	Uridine biosynthesis

Figure 2. p16/*CDKN2A* negatively correlates with mRNA and protein expression of multiple nucleotide metabolism genes. (A-B) SKMEL28 human melanoma cells were infected with lentivirus expressing a short hairpin RNA (shRNA) targeting p16 (shp16). shGFP was used as a control (shCont). **(A)** Expression of the 128 nucleotide metabolism genes from RNA-Seq. **(B)** Polysome fractionation was performed and both heavy (>2 ribosomes) and total mRNA were sequenced, and the ratio of Heavy to Total was used to assess transcripts with increased translation. **(C)** Genes that are transcriptionally or translationally upregulated in shp16 SKMEL28 cells. **(D-E)** DepMap data of cutaneous melanoma cell lines. **(D)** mRNA expression of 31 genes identified in the CRISPR screens. **(E)** Protein expression of 31 genes identified in the CRISPR screens.

Inhibition of *de novo* purine synthesis via multiple pathways decreases proliferation in shp16 cells

Our CRISPR dropout screens demonstrate that multiple nucleotide metabolism pathways may be a vulnerability of p16/Cdkn2a knockdown cells (**Fig. 1**), and further analysis indicates upregulation

A

Drug/inhibitor	Target	Pathway
Methotrexate	DHFR	Folate Cycle/1C Metabolism
Lometrexol	GART	De Novo Purine Synthesis
Aminopterin	DHFR	Folate Cycle/1C Metabolism
Mercaptopurine	Nucleotide analog	De Novo Purine Synthesis
Mycophenolic acid	IMPDH	De Novo Purine Synthesis
VX-944	IMPDH	De Novo Purine Synthesis
SHIN1	SHMT	Serine Cycle/1C Metabolism

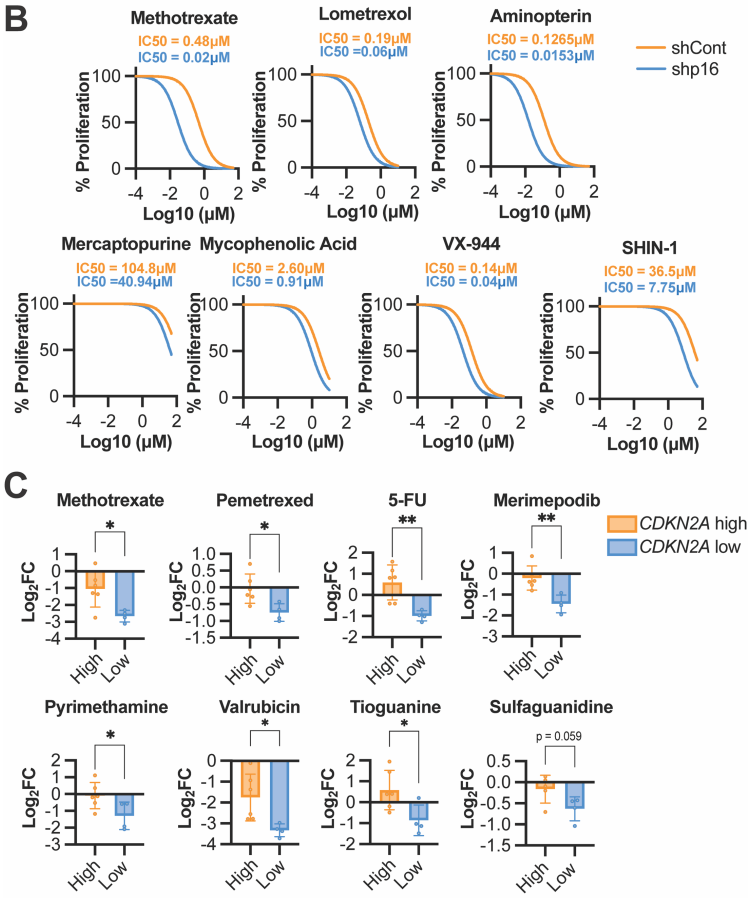

Figure 3. p16/*CDKN2A*-low cells are more sensitive to inhibitors of nucleotide metabolism. (A) Table of inhibitors used in in vitro cell line studies. 1C metabolism = one carbon metabolism. **(B)** SKMEL28 human melanoma cells were infected with lentivirus expressing a short hairpin RNA (shRNA) targeting p16 (shp16). shGFP was used as a control (shCont). Cells were treated with the indicated inhibitors and proliferation was assessed by crystal violet staining. **(C)** Increased drug sensitivity from DepMap data of cutaneous melanoma cell lines with high or low *CDKN2A* expression. *p<0.05, **p<0.01

of *de novo* purine synthesis and one carbon metabolism genes in shp16 cells (**Fig. 2**). We therefore used a variety of inhibitors that target these pathways (**Fig. 3A**). We determined that human isogenic cells with p16 knockdown are more sensitive to many of these inhibitors *in vitro* (**Fig. 3B**). Additionally, knockdown or knockout of *Cdkn2a* in mouse cells increased sensitivity to methotrexate, lometrexol, and aminopterin (**Fig. S2A-C**). We also found a correlation between *CDKN2A* expression and sensitivity to a variety of drugs that target nucleotide synthesis and antimetabolites in cutaneous melanoma cell lines on DepMap (**Fig. 3C**). Interestingly, while prior reports have demonstrated that *MTAP* deletions, which are near the same chromosomal locus as *CDKN2A*, increase sensitivity to *de novo* purine inhibitors, we did not observe decreased *MTAP* expression in our human or mouse knockdown cells (**Fig. S2D**). These data provide evidence that p16/*Cdkn2a*-low cells are overall more sensitive to inhibition of nucleotide metabolism pathways, including *de novo* purine synthesis and folate synthesis, which corroborates our *in vitro* CRISPR screens (**Fig. 1**).

Anti-folates increase apoptosis in shp16 cells

Next, we aimed to explore the mechanism of decreased proliferation in p16 knockdown cells. We observed an increase in cytotoxicity in shp16 cells treated with methotrexate and lometrexol compared to controls (**Fig. 4A**). Annexin V/PI staining was increased in shp16 cells compared to controls, suggesting these cells are undergoing apoptosis after treatment with these inhibitors (**Fig. 4B**). We did not observe an increase in senescence in shp16 cells treated with methotrexate or lometrexol, as assessed by senescence-associated beta-galactosidase staining (**Fig. S3A**). This is in contrast to the CDK4/6 inhibitor palbociclib, which induced robust senescence in shp16 cells (**Fig. S3B**). Moreover, we previously published that p16 loss suppresses factors related to the senescence-associated secretory phenotype (SASP) (Buj et al., 2021), and treatment of shp16 cells with palbociclib indeed decreased SASP expression (**Fig. S3C**). These data demonstrate

that inhibition of *de novo* purine synthesis via the folate cycle induces apoptosis and also show that inhibiting the CDK4/6 axis in p16-low cells does not increase the SASP, which has implications for using these inhibitors in tumors with low p16/*CDKN2A*.

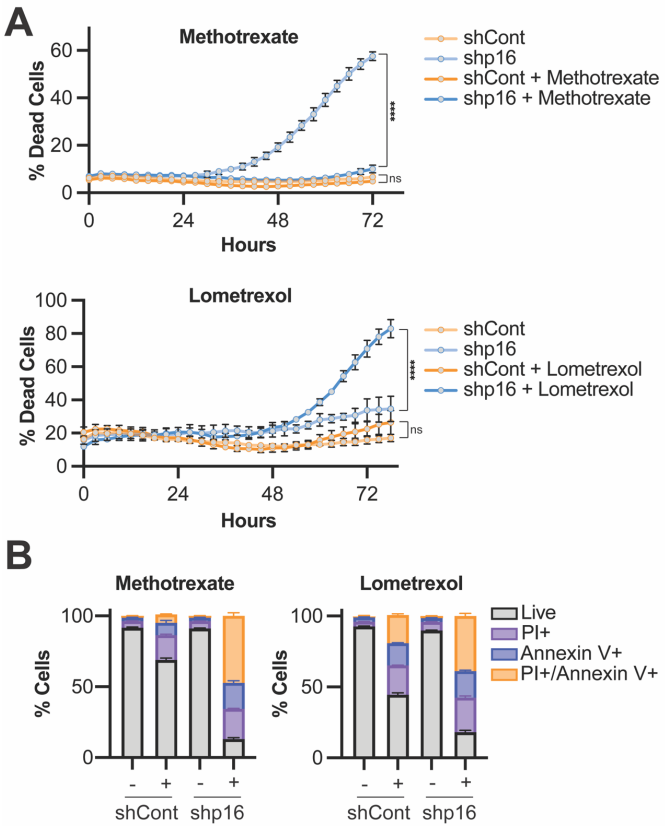

Figure 4. Multiple anti-folates induce apoptosis in p16 knockdown cells. (A-B) SKMEL28 human melanoma cells were infected with lentivirus expressing a short hairpin RNA (shRNA) targeting p16 (shp16). shGFP was used as a control (shCont). **(A)** Cells were treated with the indicated inhibitors and cytotoxicity was assessed using IncuCyte Cytotox Green reagent. **(B)** Cells were treated with the indicated inhibitors, and apoptosis was assessed using Annexin V/PI staining by flow cytometry.

De novo purine synthesis and one carbon metabolism genes correspond to worse melanoma patient survival

Using TCGA data, we found that upregulation of *de novo* purine synthesis and one carbon metabolism genes occurs in many metastatic melanomas, although *MTAP* is typically downregulated due to deletion of chromosome 9p21 (Zhang et al., 1996) (**Fig. 5A** and **Table S7**). Moreover, alteration of these genes corresponds with worse overall survival (**Fig. 5B**), whereas upregulation

of genes involved in *de novo* pyrimidine synthesis, overall nucleotide biosynthesis, or nucleotide salvage do not have an association with melanoma patient survival (**Fig. 5C-D**).

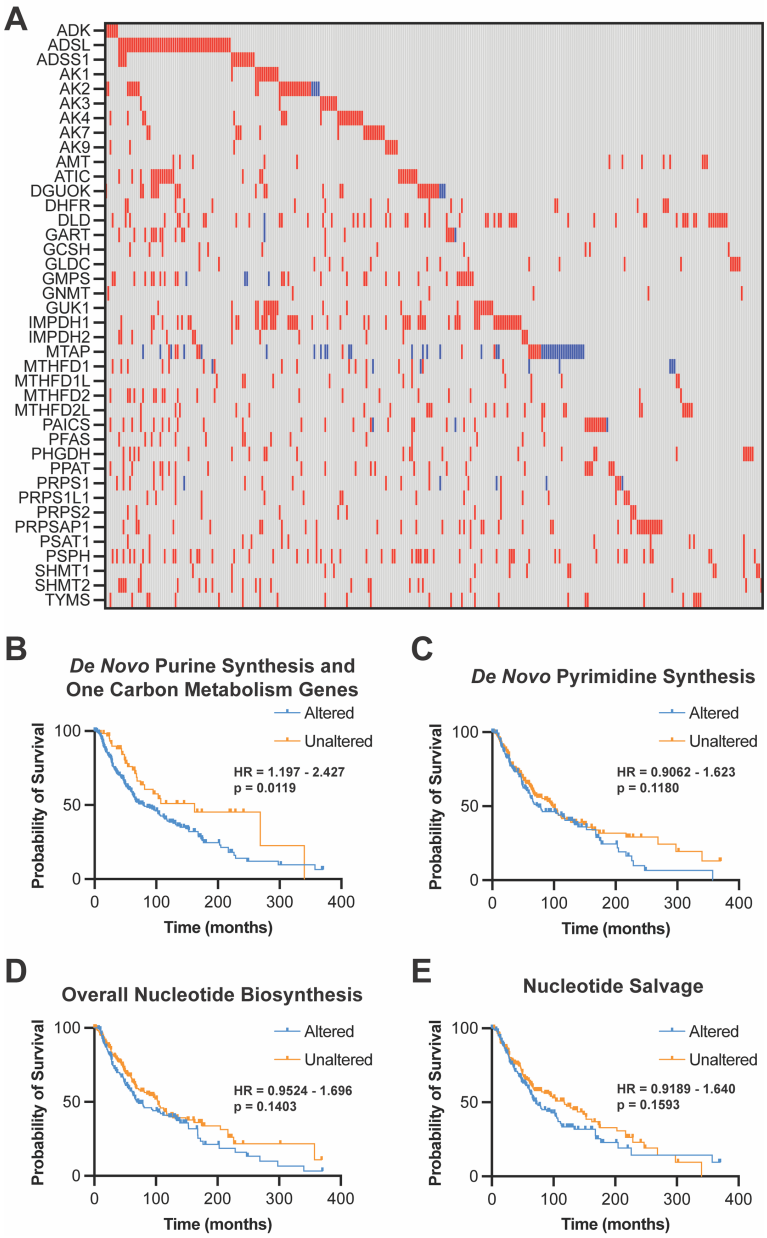

Figure 5. *De novo* purine synthesis and one carbon metabolism genes are associated with worse overall survival in metastatic melanomas. Data from The Cancer Genome Atlas (TCGA) Skin Cutaneous Melanoma PanCancer Atlas (367 metastatic melanomas). **(A)** *De novo* purine synthesis and one carbon metabolism genes in TCGA metastatic melanoma samples. Red indicates increased mRNA expression. Blue indicates decreased mRNA expression. Overall survival probability of patients with alterations in *de novo* purine synthesis and one carbon metabolism genes **(B)**, *de novo* pyrimidine genes **(C)**, overall nucleotide biosynthesis genes **(D)**, and nucleotide salvage genes **(E)**. Log rank p value.

Discussion

We previously found that p16 loss increases nucleotide synthesis via mTORC1 and the PPP (Buj et al., 2019). Here we identified multiple other nucleotide metabolic genes that are potential vulnerabilities of p16-low cells. Upon direct comparison of multiple anti-folates and anti-metabolites in p16 wildtype and shp16 cells, we found that p16 status corresponds to therapeutic response to many of these agents. These agents induce cell death, unlike the CDK4/6 inhibitor palbociclib that induces senescence. Given the context-dependent effects of senescence on the microenvironment (detailed below), these data suggest that *de novo* purine synthesis or one carbon metabolism inhibitors may provide therapeutic benefit for the ~50% of human tumors with low p16/CDKN2A expression.

Previous studies and clinical trials found that most chemotherapies have little clinical benefit in melanoma patients (Luke and Schwartz, 2013). However, to date, trials have not stratified patients based on p16 expression. Our data suggest that while patients with wildtype p16 with moderate expression would likely not robustly respond to these therapies, those with low or mutant p16 may benefit. Moreover, the *CDKN2A* gene is located on chromosome 9p21 and is often deleted in tandem with other genes in that locus including *MTAP* (Zhang et al., 1996). Prior work has found that patients with *MTAP* deletions are more responsive to *de novo* purine synthesis inhibitors, including anti-folates (Alhalabi et al., 2022; Hu et al., 2021; Tang et al., 2018), although we did not observe a decrease in MTAP upon p16 knockdown (**Fig. S2D**). Thus, cancers with homozygous deletion of the entire locus containing both genes would presumably be highly sensitive to these inhibitors, although this will need to be tested experimentally in isogenic cells. Additionally, we previously demonstrated that p16 loss increases mTORC1 activity (Buj et al., 2019), and a recent study found that cancers with increased mTORC1, such as those with TSC2 deficiency, are highly sensitive to inhibitors of IMPDH (Valvezan et al., 2020). Together, these data open up

new questions regarding the importance of stratification of patients for future anti-metabolite therapy based on p16 status.

Multiple anti-folates increased cell death in shp16 cells, although the mechanism remains to be determined. p16 knockdown cells proliferate faster than p16 wildtype cells (**Fig. S1B**). Increased proliferation would increase the demand for dNTPs and likely other nucleotides required for biomass. Indeed, many chemotherapies are more effective in highly proliferative cells, and the status of other cell cycle regulators such as RB1 and CDK12 affect response to anti-folates and anti-metabolites (Derenzini et al., 2008; Filippone et al., 2022; Robinson et al., 2013). We cannot rule out other effects of these agents, such as redox imbalance due to inhibition of glutathione synthesis or NADPH, changes in methylation due to methionine cycle dysregulation, or energy stress due to decreased ATP. Indeed, one paper has linked p16 deficiency to increased mitochondrial ROS that is uncoupled from cell cycle regulation (Tyagi et al., 2017), again suggesting a need to better understand non-canonical roles of p16 when mechanistically investigating therapies. Future work will be required to more fully elucidate the mechanisms of sensitivity, which may provide additional evidence into the metabolic reprogramming induced by p16 loss.

Melanoma standard-of-care is now immunotherapy (Larkin et al., 2015; Robert et al., 2015a; Robert et al., 2015b), although >40% of patients do not achieve a significant response (Callahan et al., 2018; Robert et al., 2015b; Valsecchi, 2015; Wolchok et al., 2017). Interestingly, recent data demonstrate that a decreased purine to pyrimidine ratio leads to a nucleotide imbalance that elevates the expression of the immunoproteasome and enhances anti-PD1 response (Keshet et al., 2020; Lee et al., 2018). Another study found that the anti-folate pemetrexed induces immunogenic cell death and augments T cell function to synergize with anti-PD1 (Schaer et al., 2019). Therefore, these inhibitors may promote an anti-tumor immune response that could be exploited in combination with immunotherapy. Indeed, multiple trials are ongoing to better understand whether

these agents can be used in combination in a variety of solid tumors, including melanoma (Lelliott et al., 2022) (clinicaltrials.gov). While these drugs are also potent immunosuppressants, our data suggest there is a therapeutic window in p16-low tumors that may allow for an anti-tumor response.

CDK4/6 inhibitors are currently in clinical trials in combination with immunotherapies in melanoma and other solid tumors (Ettl et al., 2022; Lelliott et al., 2022; Liu et al., 2020; Moore et al., 2022) (clinicaltrials.gov). These inhibitors induce cytostasis, generally associated with a senescence arrest (Klein et al., 2018). Indeed, we observed senescence in shp16 cells treated with the CDK4/6 inhibitor palbociclib (**Fig. S3B**). Induction of senescence may promote an anti-tumor immune response via the SASP (Chen et al., 2023; Hao et al., 2021; Marin et al., 2023; Paffenholz et al., 2022; Xue et al., 2007), although other studies suggest senescence and the SASP is immunosuppressive (Faget et al., 2019; Oesterreich and Aird, 2023; Shahbandi et al., 2022). We previously published that loss of p16/*CDKN2A* expression corresponds to decreased SASP (Buj et al., 2021), and our data here indicate a blunted SASP induction in p16 knockdown cells treated with palbociclib (**Fig. S3C**). This suggests that while CDK4/6 inhibitors induce a potent cytostatic effect in p16-low cells, they may not have the added benefit to potentiate immunotherapy due to suppressed pro-inflammatory factors. Experiments to determine the extent of synergy between CDK4/6 inhibitors and immunotherapy in the context of p16 expression will be helpful towards understand this combination.

In summary, we identified multiple metabolic vulnerabilities of p16-low cancer cells that can be exploited using various anti-metabolites or anti-folates. While we focused on melanoma cells in this study, these results may have implications for other human tumors where p16 expression is lost as we have previously published that metabolic changes due to p16 loss are a universal

phenomenon (Buj et al., 2019). Low expression of p16 may open up a therapeutic window for these agents that kill tumor cells, although this will need to be further investigated in humans.

Supplemental Figures

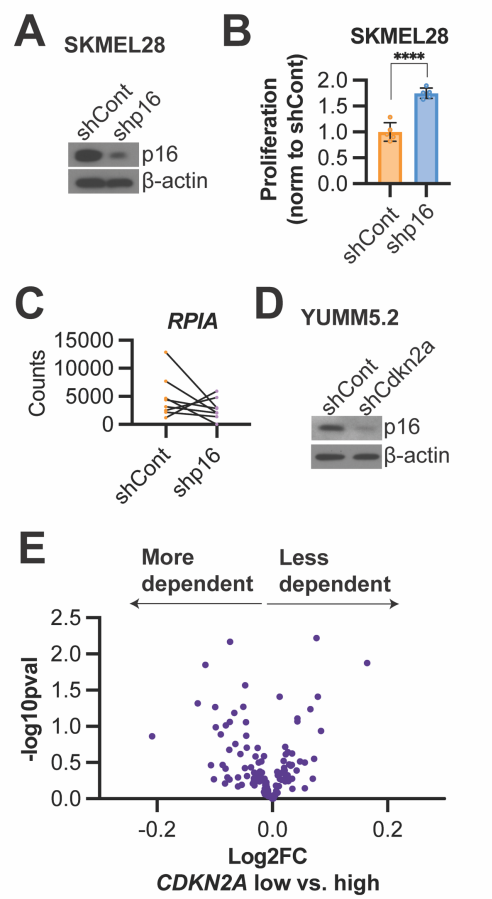

Figure S1. Knockdown of p16/*Cdkn2a* in human and mouse melanoma cell lines and Dep-Map dependency score data based on *CDKN2A* expression. Related to Figure 1. (A-B) SKMEL28 human melanoma cells were infected with lentivirus expressing a short hairpin RNA (shRNA) targeting p16 (shp16). shGFP was used as a control (shCont). **(A)** Immunoblot analysis of p16. β-actin was used as a loading control. **(B)** Proliferation was assessed by crystal violet staining. ****p<0.001 **(C)** Counts for each *RPIA* gRNA in the SKMEL28 CRISPR KO screen (**see Fig. 1B**). **(D)** Yumm5.2 mouse melanoma cells were infected with lentivirus expressing a shRNA targeting *Cdkn2a* (shCdkn2a). shGFP was used as a control (shCont). Immunoblot analysis of p16. β-actin was used as a loading control. **(E)** Volcano plot of dependency data from DepMap of cutaneous melanoma cell lines based on *CDKN2A* expression.

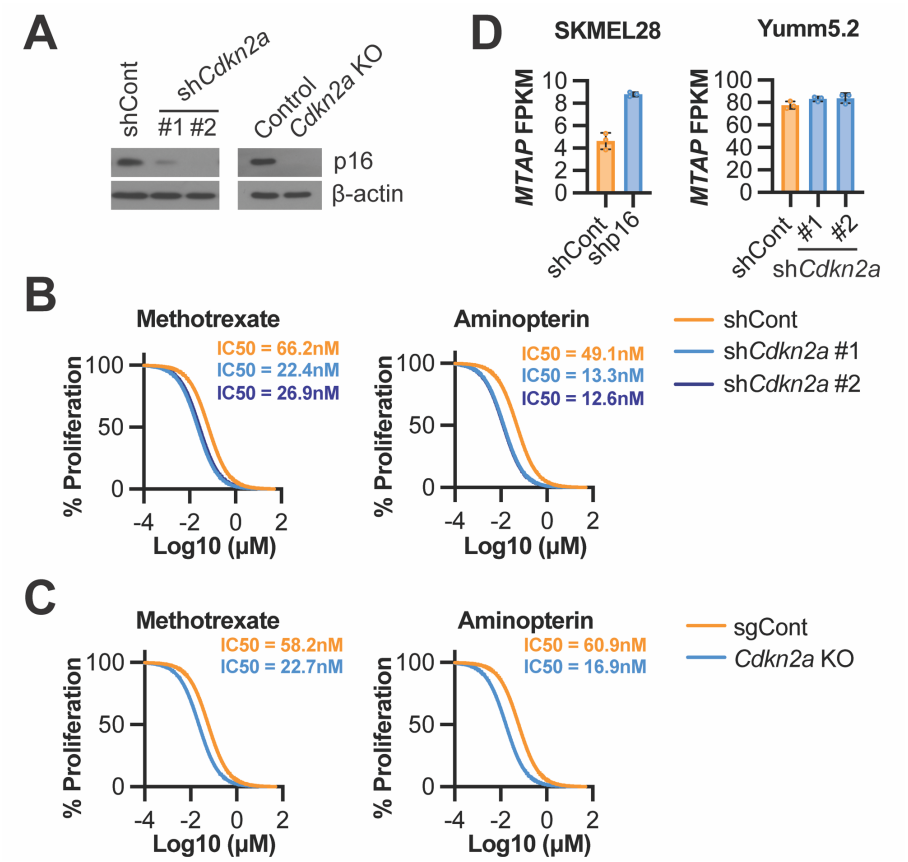

Figure S2. Knockdown or knockout of Cdkn2a in mouse melanoma cell lines increases sensitivity to multiple anti-folates. Related to Figure 2. (A-B) Yumm5.2 mouse melanoma cells were infected with lentivirus expressing short hairpin RNAs (shRNA) targeting *Cdkn2a* (sh*Cdkn2a* #1 and #2) or a gRNA targeting *Cdkn2a*. shGFP was used as a control for KD experiments (shCont). A gRNA targeting an intergenic region was used as a control for KO experiments. **(A)** Immunoblot analysis of p16. β-actin was used as a loading control. **(B-C)** Cells were treated with the indicated inhibitors, and proliferation was assessed by crystal violet staining. **(D)** *MTAP* Fragments Per Kilobase of transcript per Million mapped reads (FPKM) in SKMEL28 human melanoma cells with p16 knockdown (shp16) and Yumm5.2 mouse melanoma cells with *Cdkn2a* knockdown (sh*Cdkn2a* #1 and #2).

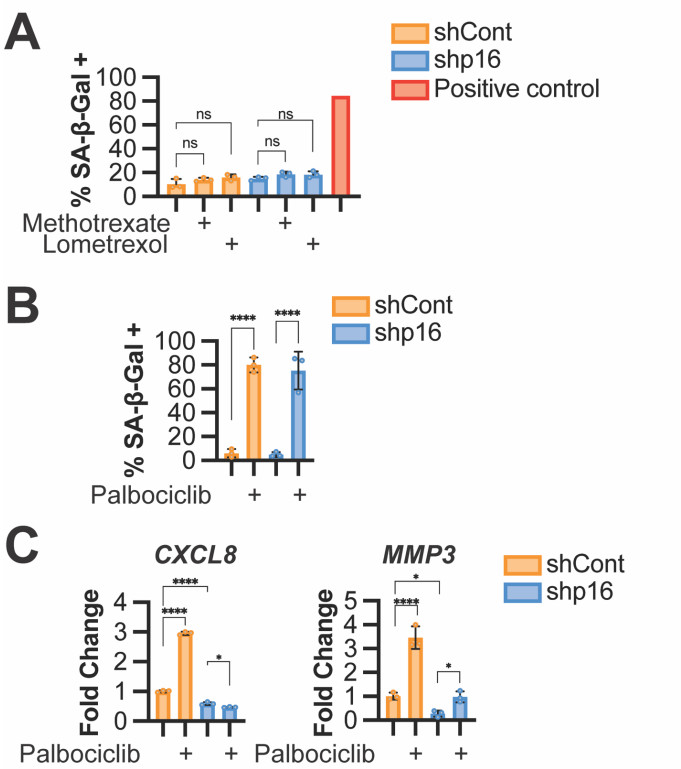

Figure S3. Anti-folates do not induce senescence; and shp16 cells do not mount a robust senescence-associated secretory phenotype (SASP) in response to palbociclib. Related to Figure 4. (A-C) SKMEL28 human melanoma cells were infected with lentivirus expressing a short hairpin RNA (shRNA) targeting p16 (shp16). shGFP was used as a control (shCont). **(A)** Cells were treated with the indicated inhibitors, and senescence-associated beta-galactosidase (SA-β-Gal) was assessed. Cisplatin was used as a positive control. **(B-C)** Cells were treated with 1μM palbociclib. **(B)** SA-β-Gal staining. **(C)** SASP gene expression. ****p<0.001; ns = not significant

Acknowledgments

This work was supported by grants from the National Institutes of Health (R37CA240625 to K.M.A. and T32GM133332 to A.R.C.) and the Melanoma Research Foundation (to R.B.G.). This project used the following Hillman Cancer Center Flow Facility, Cancer Bioinformatics Services, and Cancer Genomics Facility shared resources which are supported in part by award P30CA047904.

Author Contributions

Naveen Kumar Tangudu: Investigation, Methodology, Visualization, Writing – Review & Editing. **Raquel Buj:** Investigation, Visualization, Writing – Review & Editing. **Jiefei Wang:** Software, Formal Analysis. **Aidan Cole:** Investigation, Writing – Review & Editing. **Apoorva Uboveja:** Investigation, Writing – Review & Editing. **Richard Fang:** Investigation. **Amandine Amalric:** Investigation, Writing – Review & Editing. **Maureen A. Lyons:** Methodology. **Uma R. Chandran:** Methodology, Supervision. **Katherine M. Aird:** Conceptualization, Visualization, Writing – Original Draft, Writing – Review & Editing, Supervision, Project Administration, Funding Acquisition.

Declaration of Interests

The authors declare no competing interests.

Methods

Cell Lines

SKMEL28 and Yumm5.2 cells were purchased from ATCC. SKMEL28 cells were cultured in DMEM (MT10013CV, Fisher Scientific). Yumm5.2 cells were cultured in DMEM (MT10092CV, Fisher Scientific). Both were supplemented with 5% Fetal Bovine Serum (S1620, BioWest) and 1% Penicillin/Streptomycin (15-140-122, Fisher Scientific). All cell lines were routinely tested for mycoplasma as described in (Uphoff and Drexler, 2005).

Lentiviral packaging and infection

The human shRNA hairpin pLKO.1-shp16 (TRCN0000010482), the murine shRNA hairpins pLKO.1-shCdkn2a #1 (TRCN0000077816) and #2 (TRCN0000362595) and the human and murine pLKO.1-shGFP control (Addgene, cat#30323) vectors were packaged using the ViraPower Kit (Invitrogen, cat#K497500) following the manufacturer's instructions. Cells were infected with corresponding vectors for 16h and selected for 3 days with 1µg/mL of puromycin (SKMEL28) or 3µg/mL puromycin (YUMM5.2).

Design of *Cdkn2a* CRISPR KO murine cell line

Single-stranded oligonucleotides targeting *CDKN2A* (forward: CACCGGCTG-GATGTGCGCGATGCC and reverse: AAACGGCATCGCGCACATCCAGCC, Integrated DNA Technologies) or intergenic region control (forward: CACCGAGTGTTCCTAGAGATAGAAG and reverse: AAACCTTCTATCTCTCTAGGAACACTC) were annealed, phosphorylated, and ligated into pLentiCRISPRv2 (Addgene cat#52961), kindly gifted by Feng Zhang. Lentivirus was packaged using the ViraPower Kit as described above and used to infect YUMM5.2 cells. Mixed pooled

population YUMM5.2 cells infected with intergenic region control gRNAs were used as control while a single clone was obtained for YUMM5.2 cells targeted with *CDKN2A* gRNAs.

Nucleotide Metabolic CRISPR library construction

We constructed a pooled sgRNA library containing 2800 sgRNAs targeting various genes either directly or indirectly related to nucleotide metabolism in addition to controls targeting intragenic regions as described previously (Joung et al., 2017). Briefly, we used publicly available CRISPR sgRNA design tools that optimize on-target and minimize off-target genome editing (http://crispr.dfci.harvard.edu/SSC/) and pooled human metabolic library (Birsoy et al., 2015) to identify 10 sgRNAs for each gene. The pooled oligo library was synthesized by Twist Bioscience. To the oligo library was cloned into lentiCRISPRv2, Addgene 52961) by PCR amplification using NEB Next High-Fidelity PCR Master Mix (New England Biolabs, M0541S). The PCR product was digested with Esp3I (BsmBI) (Fisher Scientific, FERFD0454) and ligated into the cut lentiCRIS-PRv2 backbone. The library was sequenced prior to its use to confirm coverage.

CRISPR-based Screens

The human nucleotide-focused CRISPR KO library containing 128 genes involved in nucleotide biosynthesis, salvage, and catabolism (Table S1), was designed as stated above. The mouse metabolic-focused CRISPR KO library was a gift from Dr. Kivanc Birsoy (Addgene #160129). The screening using the human nucleotide-focused library was conducted on SKMEL28 shGFP control and shp16 cells, while the screening using the mouse metabolic-focused library was conducted on YUMM5.2 shGFP control and shCdkn2a #1 cells. Briefly, the appropriate number of cells were infected with pooled libraries at an MOI <0.3 to achieve >400-fold library coverage after selection with puromycin. Cells were passaged every 2-3 days for two weeks maintaining the

whole population. At the end of the experiments, cells were harvested for genomic DNA extraction using the Zymo Research kit (cat# D4069). sgRNA inserts were PCR amplified using Ex Taq DNA Polymerase (Takara cat#RR001A) from sufficient genome equivalents of DNA to achieve an average coverage of >200x of the sgRNA library. See primers in **Table S8**. Pooled PCR amplicons were then sequenced. MAGeCK was used as the bioinformatics pipeline to analyze negatively and positively enriched genes(Li et al., 2014).

Western blotting

Cells lysates were collected in 1X sample buffer (2% SDS, 10% glycerol, 0.01% bromophenol blue, 62.5mM Tris, pH 6.8, 0.1M DTT) and boiled to 95°C for 10 min. Protein concentration was determined using the Bradford assay. An equal amount of total protein was resolved using SDS-PAGE gels and transferred to nitrocellulose membranes (Fisher Scientific) at 110mA for 2h at 4°C. Membranes were blocked with 5% nonfat milk or 4% BSA in TBS containing 0.1% Tween-20 (TBS-T) for 1 h at room temperature. Membranes were incubated overnight at 4°C in primary antibodies in 4% BSA/TBS + 0.025% sodium azide. Membranes were washed 4 times in TBS-T for 5 min at room temperature after which they were incubated with HRP-conjugated secondary antibodies (Cell Signaling, Danvers, MA) for 1 h at room temperature. After washing 4 times in TBS-T for 5 min at room temperature, proteins were visualized on film after incubation with SuperSignal West Pico PLUS Chemiluminescent Substrate (ThermoFisher, Waltham, MA). Primary antibodies: Rabbit anti-CDKN2A (Abcam, ab108349; 1:1000); Rabbit anti-p16 INK4A (Cell Signaling Technology, 29271; 1:1000); Rabbit anti-CDKN2A/p19 ARF (Abcam, ab80; 1:1000); mouse anti-β-actin (Sigma Aldrich, A1978; 1:10000). Secondary antibodies: Anti-mouse IgG, HRP-linked (Cell Signaling Technology, 7076; 1:10,000), Anti-Rabbit IgG, HRP-linked (Cell Signaling Technology, 7074; 1:5000).

Proliferation assays

An equal number of cells were seeded in multiwell plates and cultured for 4-5 days. Proliferation was assessed by fixing the plates for 5 min with 1% paraformaldehyde after which they were stained with 0.05% crystal violet. Wells were destained using 10% acetic acid. Absorbance (590nm) was measured using a spectrophotometer (BioTek Epoch Microplate reader).

RNA isolation, Sequencing, and Analysis

Total RNA was extracted from cells with Triol (Ambion, cat#15596018) and DNase treated, cleaned and concentrated using Zymo columns (Zymo Research, cat#R1013) following manufacturer's instructions. RNA integrity number (RIN) was measured using BioAnalyzer (Agilent Technologies) RNA 6000 Nano Kit to confirm RIN above 7 for each sample. The cDNA libraries, next generation sequencing, and bioinformatics analysis was performed by Novogene.

Polysome Profiling and Sequencing

Eight culture plates per condition (~23 million cells per condition) were incubated with harringtonine (2μg/mL) for 2 minutes at 37ºC followed by 5 minutes of cycloheximide (100μg/mL) treatment at 37ºC. Cells were washed twice with PBS after each treatment. Cells were scraped in 600uL of lysis buffer (50mM HEPES, 75mM KCl, 5mM MgCl2, 250mM sucrose, 0.1mg/mL cycloheximide, 2mM DTT, 1% Triton X-100 and 1.3% sodium deoxycholate and 5μl of RNase OUT) on ice. Lysates were rocked for 10 minutes at 4ºC and centrifuged at 3000g for 15 minutes at 4ºC. 400μl of lysates supernatant (cytosolic cell extracts) were layered over cold sucrose gradients (10mM HEPES, 75mM KCl, 5mM MgCl2, 0.5mM EDTA and increasing sucrose concentrations from 20% to 47%). Gradients were centrifuged at 34,000 rpms in a Beckman SW41 rotor for 2h and 40 minutes at 4ºC. After centrifugation, low (0 to 2 ribosomes) and high (>2 ribosomes) polysome fractions were collected in Trizol (1:1) using a density gradient fractionation system

(Brandel) equipped with a UA-6 absorbance detector and a R1 fraction collector. RNA was DNase treated, cleaned, and concentrated using Zymo columns (Zymo Research, Cat# R1013). The cDNA libraries, next generation sequencing, and bioinformatics analysis was performed by Novogene.

Dependency Map Data

For analysis of dependency scores, CRISPR (DepMap Public 23Q2+Score, Chronos) was downloaded for cutaneous melanoma cell lines. Cells were characterized as *CDKN2A* high or low based on mRNA expression (Expression Public 23Q2). Cell lines with known CDKN2A mutations were excluded. A similar method was used to analyze proteomics and drug sensitivity (using the PRISM Repurposing Primary Screen).

IncuCyte cytotoxicity assay

Live cell viability was assessed using IncuCyte S3 imaging system (Sartorius). Briefly, cells were seeded in 96 well plate and treated with drug, either methotrexate (13960; Cayman Chemical Company) or lometrexol hydrate (18049; Cayman Chemical Company), in the presence of 1x Cytotox green reagent (ESS4633; Sartorius), a highly sensitive cyanine nucleic acid dye. Cells were imaged for 3 days with live cell imaging every 3h point. Dead cell quantification was performed using the IncuCyte software.

Annexin V/propidium iodide staining and flow cytometry

For Annexin V/7AAD experiments, cells (4×10^4/well in 6-well plates) were treated for 5 days with 0.07μM methotrexate or 0.09μM lometrexol in DMEM + 5% FBS. Cells were trypsinized, counted in hemocytometer, and each FACS tube contained approximately 2×10^5 harvested cells. Cells were stained with Annexin V (R37176; Thermo Fisher Scientific) in 2.5 mM Ca2+ containing

DMEM for 15 min at room temperature. Prior to FACS analysis, 5µl (40ng/sample) propidium iodide added to cell suspension (00-6990-50; eBiosciences). Data were analyzed using FlowJo software. Single stain controls were used for compensation.

RT-qPCR of SASP genes:

Cells were treated with 1µM palbociclib for 5 days. RNA was retrotranscribed with High-Capacity cDNA Reverse Transcription Kit (Applied Biosystems, cat#4368814) and 20ng of cDNA amplified using the CFX Connect Real-time PCR system (Bio-Rad) and the PowerUp™ SYBR™ Green Master Mix (Applied Biosystems, cat#A25742) following manufacturer's instructions. Primers were designed using the Integrated DNA Technologies (IDT) web tool (**Table S8**). Conditions for amplification were: 5 min at 95° C, 40 cycles of 10 sec at 95° C and 7 sec at 62° C. The assay ended with a melting curve program: 15 sec at 95° C, 1 min at 70° C, then ramping to 95° C while continuously monitoring fluorescence. Each sample was assessed in triplicate. Relative quantification was determined to multiple reference genes (human: PSMC4, and B2M and mouse: Rplp0 and Gusb) to ensure reproducibility using the delta-delta CT method.

Senescence Associated-β-Galactosidase assay:

Cells were treated with 1µM palbociclib for 5 days. SA-β-Gal staining was performed as previously described (Dimri et al., 1995). Cells were fixed in 2% formaldehyde/0.2% glutaraldehyde in PBS (5 min) and stained (40 mM Na_2HPO_4, 150 mM NaCl, 2 mM $MgCl_2$, 5 mM $K_3Fe(CN)_6$, 5 mM $K_4Fe(CN)_6$, and 1 mg/ml X-gal) overnight at 37°C in a non-CO2 incubator. Images were acquired at room temperature using an inverted microscope (Nikon Eclipse Ts2) with a 20X/0.40 objective (Nikon LWD) equipped with a camera (Nikon DS-Fi3). Each sample was assessed in triplicate and at least 100 cells per well were counted (> 300 cells per experiment).

Analysis of The Cancer Genome Atlas patient data

Data were extracted from The Cancer Genome Atlas (TCGA) Skin Cutaneous Melanoma Pan-Cancer Atlas (367 metastatic melanomas) using cBioportal survival analysis. Overall survival probability and hazard ratios were calculated using the Log rank statistical test.

Quantification and Statistical Analysis

GraphPad Prism version 9.0 was used to perform statistical analysis. The appropriate statistical test was used as indicated to determine p values of raw data. P-values < 0.05 were considered significant.

References

Aird, K.M., and R. Zhang. 2015. Nucleotide metabolism, oncogene-induced senescence and cancer. *Cancer letters*. 356:204-210.

Alhalabi, O., J. Chen, Y. Zhang, Y. Lu, Q. Wang, S. Ramachandran, R.S. Tidwell, G. Han, X. Yan, J. Meng, R. Wang, A.G. Hoang, W.L. Wang, J. Song, L. Lopez, A. Andreev-Drakhlin, A. Siefker-Radtke, X. Zhang, W.F. Benedict, A.Y. Shah, J. Wang, P. Msaouel, M. Zhang, C.C. Guo, B. Czerniak, C. Behrens, L. Soto, V. Papadimitrakopoulou, J. Lewis, W. Rinsurongkawong, V. Rinsurongkawong, J. Lee, J. Roth, S. Swisher, I. Wistuba, J. Heymach, J. Wang, M.T. Campbell, E. Efstathiou, M. Titus, C.J. Logothetis, T.H. Ho, J. Zhang, L. Wang, and J. Gao. 2022. MTAP deficiency creates an exploitable target for antifolate therapy in 9p21-loss cancers. *Nature communications*. 13:1797.

Ali, E.S., and I. Ben-Sahra. 2023. Regulation of nucleotide metabolism in cancers and immune disorders. *Trends Cell Biol*.

Birsoy, K., T. Wang, W.W. Chen, E. Freinkman, M. Abu-Remaileh, and D.M. Sabatini. 2015. An Essential Role of the Mitochondrial Electron Transport Chain in Cell Proliferation Is to Enable Aspartate Synthesis. *Cell*. 162:540-551.

Buj, R., and K.M. Aird. 2018. Deoxyribonucleotide Triphosphate Metabolism in Cancer and Metabolic Disease. *Frontiers in endocrinology*. 9:177.

Buj, R., and K.M. Aird. 2019. p16: cycling off the beaten path. *Molecular & Cellular Oncology*. 6:e1677140.

Buj, R., C.W. Chen, E.S. Dahl, K.E. Leon, R. Kuskovsky, N. Maglakelidze, M. Navaratnarajah, G. Zhang, M.T. Doan, H. Jiang, M. Zaleski, L. Kutzler, H. Lacko, Y. Lu, G.B. Mills, R. Gowda, G.P. Robertson, J.I. Warrick, M. Herlyn, Y. Imamura, S.R. Kimball, D.J. DeGraff, N.W. Snyder, and K.M. Aird. 2019. Suppression of p16 Induces mTORC1-Mediated Nucleotide Metabolic Reprogramming. *Cell reports*. 28:1971-1980.e1978.

Buj, R., K.E. Leon, M.A. Anguelov, and K.M. Aird. 2021. Suppression of p16 alleviates the senescence-associated secretory phenotype. *Aging (Albany NY)*. 13:3290-3312.

Callahan, M.K., H. Kluger, M.A. Postow, N.H. Segal, A. Lesokhin, M.B. Atkins, J.M. Kirkwood, S. Krishnan, R. Bhore, C. Horak, J.D. Wolchok, and M. Sznol. 2018. Nivolumab Plus Ipilimumab in Patients With Advanced Melanoma: Updated Survival, Response, and Safety Data in a Phase I Dose-Escalation Study. *J Clin Oncol*. 36:391-398.

Chen, H.A., Y.J. Ho, R. Mezzadra, J.M. Adrover, R. Smolkin, C. Zhu, K. Woess, N. Bernstein, G. Schmitt, L. Fong, W. Luan, A. Wuest, S. Tian, X. Li, C. Broderick, R.C. Hendrickson, M. Egeblad, Z. Chen, D. Alonso-Curbelo, and S.W. Lowe. 2023. Senescence Rewires Microenvironment Sensing to Facilitate Antitumor Immunity. *Cancer discovery*. 13:432-453.

Derenzini, M., G. Donati, G. Mazzini, L. Montanaro, M. Vici, C. Ceccarelli, D. Santini, M. Taffurelli, and D. Treré. 2008. Loss of retinoblastoma tumor suppressor protein makes human breast cancer cells more sensitive to antimetabolite exposure. *Clin Cancer Res*. 14:2199-2209.

Dimri, G.P., X. Lee, G. Basile, M. Acosta, G. Scott, C. Roskelley, E.E. Medrano, M. Linskens, I. Rubelj, O. Pereira-Smith, and et al. 1995. A biomarker that identifies senescent human cells in culture and in aging skin in vivo. *Proceedings of the National Academy of Sciences of the United States of America*. 92:9363-9367.

Esteller, M., P.G. Corn, S.B. Baylin, and J.G. Herman. 2001. A gene hypermethylation profile of human cancer. *Cancer Res*. 61:3225-3229.

Ettl, T., D. Schulz, and R.J. Bauer. 2022. The Renaissance of Cyclin Dependent Kinase Inhibitors. *Cancers*. 14.

Faget, D.V., Q. Ren, and S.A. Stewart. 2019. Unmasking senescence: context-dependent effects of SASP in cancer. *Nature reviews. Cancer*. 19:439-453.

Filippone, M.G., D. Gaglio, R. Bonfanti, F.A. Tucci, E. Ceccacci, R. Pennisi, M. Bonanomi, G. Jodice, M. Tillhon, F. Montani, G. Bertalot, S. Freddi, M. Vecchi, A. Taglialatela, M. Romanenghi, F. Romeo, N. Bianco, E. Munzone, F. Sanguedolce, G. Vago, G. Viale, P.P. Di Fiore, S. Minucci, L. Alberghina, M. Colleoni, P. Veronesi, D. Tosoni, and S. Pece. 2022. CDK12 promotes tumorigenesis but induces vulnerability to therapies inhibiting folate one-carbon metabolism in breast cancer. *Nature communications*. 13:2642.

Garutti, M., G. Targato, S. Buriolla, L. Palmero, A.M. Minisini, and F. Puglisi. 2021. CDK4/6 Inhibitors in Melanoma: A Comprehensive Review. *Cells*. 10.

Hao, X., B. Zhao, W. Zhou, H. Liu, T. Fukumoto, D. Gabrilovich, and R. Zhang. 2021. Sensitization of ovarian tumor to immune checkpoint blockade by boosting senescence-associated secretory phenotype. *iScience*. 24:102016.

Hu, Q., Y. Qin, S. Ji, X. Shi, W. Dai, G. Fan, S. Li, W. Xu, W. Liu, M. Liu, Z. Zhang, Z. Ye, Z. Zhou, J. Yang, Q. Zhuo, X. Yu, M. Li, and X. Xu. 2021. MTAP Deficiency-Induced Metabolic Reprogramming Creates a Vulnerability to Cotargeting De Novo Purine Synthesis and Glycolysis in Pancreatic Cancer. *Cancer research*. 81:4964-4980.

Inoue, K., and E.A. Fry. 2018. Aberrant expression of p16(INK4a) in human cancers - a new biomarker? *Cancer Rep Rev*. 2.

Joung, J., S. Konermann, J.S. Gootenberg, O.O. Abudayyeh, R.J. Platt, M.D. Brigham, N.E. Sanjana, and F. Zhang. 2017. Genome-scale CRISPR-Cas9 knockout and transcriptional activation screening. *Nature protocols*. 12:828-863.

Keshet, R., J.S. Lee, L. Adler, M. Iraqi, Y. Ariav, L.Q.J. Lim, S. Lerner, S. Rabinovich, R. Oren, R. Katzir, H. Weiss Tishler, N. Stettner, O. Goldman, H. Landesman, S. Galai, Y. Kuperman, Y. Kuznetsov, A. Brandis, T. Mehlman, S. Malitsky, M. Itkin, S.E. Koehler, Y. Zhao, K. Talsania, T.W. Shen, N. Peled, I. Ulitsky, A. Porgador, E. Ruppin, and A. Erez. 2020. Targeting purine synthesis in ASS1-expressing tumors enhances the response to immune checkpoint inhibitors. *Nat Cancer*. 1:894-908.

Klein, M.E., M. Kovatcheva, L.E. Davis, W.D. Tap, and A. Koff. 2018. CDK4/6 Inhibitors: The Mechanism of Action May Not Be as Simple as Once Thought. *Cancer cell*. 34:9-20.

Kohnken, R., K.M. Kodigepalli, and L. Wu. 2015. Regulation of deoxynucleotide metabolism in cancer: novel mechanisms and therapeutic implications. *Molecular cancer*. 14:176.

Lane, A.N., and T.W. Fan. 2015. Regulation of mammalian nucleotide metabolism and biosynthesis. *Nucleic acids research*. 43:2466-2485.

Larkin, J., V. Chiarion-Sileni, R. Gonzalez, J.J. Grob, C.L. Cowey, C.D. Lao, D. Schadendorf, R. Dummer, M. Smylie, P. Rutkowski, P.F. Ferrucci, A. Hill, J. Wagstaff, M.S. Carlino, J.B. Haanen, M. Maio, I. Marquez-Rodas, G.A. McArthur, P.A. Ascierto, G.V. Long, M.K. Callahan, M.A. Postow, K. Grossmann, M. Sznol, B. Dreno, L. Bastholt, A. Yang, L.M. Rollin, C. Horak, F.S. Hodi, and J.D. Wolchok. 2015. Combined Nivolumab and Ipilimumab or Monotherapy in Untreated Melanoma. *N Engl J Med*. 373:23-34.

Lee, J.S., L. Adler, H. Karathia, N. Carmel, S. Rabinovich, N. Auslander, R. Keshet, N. Stettner, A. Silberman, L. Agemy, D. Helbling, R. Eilam, Q. Sun, A. Brandis, S. Malitsky, M. Itkin, H. Weiss, S. Pinto, S. Kalaora, R. Levy, E. Barnea, A. Admon, D. Dimmock, N. Stern-Ginossar, A. Scherz, S.C.S. Nagamani, M. Unda, D.M. Wilson, 3rd, R. Elhasid, A. Carracedo, Y. Samuels, S. Hannenhalli, E. Ruppin, and A. Erez. 2018. Urea Cycle Dysregulation Generates Clinically Relevant Genomic and Biochemical Signatures. *Cell*. 174:1559-1570.e1522.

Lelliott, E.J., K.E. Sheppard, and G.A. McArthur. 2022. Harnessing the immunotherapeutic potential of CDK4/6 inhibitors in melanoma: is timing everything? *NPJ Precis Oncol*. 6:26.

Li, W., H. Xu, T. Xiao, L. Cong, M.I. Love, F. Zhang, R.A. Irizarry, J.S. Liu, M. Brown, and X.S. Liu. 2014. MAGeCK enables robust identification of essential genes from genome-scale CRISPR/Cas9 knockout screens. *Genome Biology*. 15:554.

Liu, Z.B., L. Zhang, J. Bian, and J. Jian. 2020. Combination Strategies of Checkpoint Immunotherapy in Metastatic Breast Cancer. *Onco Targets Ther*. 13:2657-2666.

Luke, J.J., and G.K. Schwartz. 2013. Chemotherapy in the management of advanced cutaneous malignant melanoma. *Clin Dermatol*. 31:290-297.

Marin, I., O. Boix, A. Garcia-Garijo, I. Sirois, A. Caballe, E. Zarzuela, I. Ruano, C.S. Attolini, N. Prats, J.A. López-Domínguez, M. Kovatcheva, E. Garralda, J. Muñoz, E. Caron, M. Abad, A. Gros, F. Pietrocola, and M. Serrano. 2023. Cellular Senescence Is Immunogenic and Promotes Antitumor Immunity. *Cancer discovery*. 13:410-431.

Moore, E.K., M. Strazza, and A. Mor. 2022. Combination Approaches to Target PD-1 Signaling in Cancer. *Frontiers in immunology*. 13:927265.

Oesterreich, S., and K.M. Aird. 2023. Senescence and Immunotherapy: Redundant Immunomodulatory Pathways Promote Resistance. *Cancer Immunol Res*. 11:401-404.

Paffenholz, S.V., C. Salvagno, Y.J. Ho, M. Limjoco, T. Baslan, S. Tian, A. Kulick, E. de Stanchina, J.E. Wilkinson, F.M. Barriga, D. Zamarin, J.R. Cubillos-Ruiz, J. Leibold, and S.W. Lowe. 2022. Senescence induction dictates response to chemo- and immunotherapy in preclinical models of ovarian cancer. *Proceedings of the National Academy of Sciences of the United States of America*. 119.

Robert, C., G.V. Long, B. Brady, C. Dutriaux, M. Maio, L. Mortier, J.C. Hassel, P. Rutkowski, C. McNeil, E. Kalinka-Warzocha, K.J. Savage, M.M. Hernberg, C. Lebbe, J. Charles, C. Mihalcioiu, V. Chiarion-Sileni, C. Mauch, F. Cognetti, A. Arance, H. Schmidt, D. Schadendorf, H. Gogas, L. Lundgren-Eriksson, C. Horak, B. Sharkey, I.M. Waxman, V. Atkinson, and P.A. Ascierto. 2015a. Nivolumab in previously untreated melanoma without BRAF mutation. *N Engl J Med*. 372:320-330.

Robert, C., J. Schachter, G.V. Long, A. Arance, J.J. Grob, L. Mortier, A. Daud, M.S. Carlino, C. McNeil, M. Lotem, J. Larkin, P. Lorigan, B. Neyns, C.U. Blank, O. Hamid, C. Mateus, R. Shapira-Frommer, M. Kosh, H. Zhou, N. Ibrahim, S. Ebbinghaus, A. Ribas, and K.-. investigators. 2015b. Pembrolizumab versus Ipilimumab in Advanced Melanoma. *N Engl J Med*. 372:2521-2532.

Robinson, T.J., J.C. Liu, F. Vizeacoumar, T. Sun, N. Maclean, S.E. Egan, A.D. Schimmer, A. Datti, and E. Zacksenhaus. 2013. RB1 status in triple negative breast cancer cells dictates response to radiation treatment and selective therapeutic drugs. *PloS one*. 8:e78641.

Ruas, M., S. Brookes, N.Q. McDonald, and G. Peters. 1999. Functional evaluation of tumour-specific variants of p16INK4a/CDKN2A: correlation with protein structure information. *Oncogene*. 18:5423-5434.

Schaer, D.A., S. Geeganage, N. Amaladas, Z.H. Lu, E.R. Rasmussen, A. Sonyi, D. Chin, A. Capen, Y. Li, C.M. Meyer, B.D. Jones, X. Huang, S. Luo, C. Carpenito, K.D. Roth, A. Nikolayev, B. Tan, M. Brahmachary, K. Chodavarapu, F.C. Dorsey, J.R. Manro, T.N. Doman, G.P. Donoho, D. Surguladze, G.E. Hall, M. Kalos, and R.D. Novosiadly. 2019. The Folate Pathway Inhibitor Pemetrexed Pleiotropically Enhances Effects of Cancer Immunotherapy. *Clin Cancer Res*. 25:7175-7188.

Shahbandi, A., F.Y. Chiu, N.A. Ungerleider, R. Kvadas, Z. Mheidly, M.J.S. Sun, D. Tian, D.A. Waizman, A.Y. Anderson, H.L. Machado, Z.F. Pursell, S.G. Rao, and J.G. Jackson. 2022. Breast cancer cells survive chemotherapy by activating targetable immune-modulatory programs characterized by PD-L1 or CD80. *Nat Cancer*. 3:1513-1533.

Sherr, C.J. 2001. The INK4a/ARF network in tumour suppression. *Nature reviews. Molecular cell biology*. 2:731-737.

Shi, D.D., M.R. Savani, K.G. Abdullah, and S.K. McBrayer. 2023. Emerging roles of nucleotide metabolism in cancer. *Trends in cancer*.

Tang, B., H.O. Lee, S.S. An, K.Q. Cai, and W.D. Kruger. 2018. Specific Targeting of MTAP-Deleted Tumors with a Combination of 2'-Fluoroadenine and 5'-Methylthioadenosine. *Cancer research*. 78:4386-4395.

Tong, X., F. Zhao, and C.B. Thompson. 2009. The molecular determinants of de novo nucleotide biosynthesis in cancer cells. *Curr Opin Genet Dev*. 19:32-37.

Turgeon, M.O., N.J.S. Perry, and G. Poulogiannis. 2018. DNA Damage, Repair, and Cancer Metabolism. *Frontiers in oncology*. 8:15.

Tyagi, E., B. Liu, C. Li, T. Liu, J. Rutter, and D. Grossman. 2017. Loss of p16(INK4A) stimulates aberrant mitochondrial biogenesis through a CDK4/Rb-independent pathway. *Oncotarget*. 8:55848-55862.

Uphoff, C.C., and H.G. Drexler. 2005. Detection of mycoplasma contaminations. *Methods in molecular biology (Clifton, N.J.)*. 290:13-23.

Valsecchi, M.E. 2015. Combined Nivolumab and Ipilimumab or Monotherapy in Untreated Melanoma. *N Engl J Med*. 373:1270.

Valvezan, A.J., M.C. McNamara, S.K. Miller, M.E. Torrence, J.M. Asara, E.P. Henske, and B.D. Manning. 2020. IMPDH inhibitors for antitumor therapy in tuberous sclerosis complex. *JCI insight*. 5.

Wolchok, J.D., V. Chiarion-Sileni, R. Gonzalez, P. Rutkowski, J.J. Grob, C.L. Cowey, C.D. Lao, J. Wagstaff, D. Schadendorf, P.F. Ferrucci, M. Smylie, R. Dummer, A. Hill, D. Hogg, J. Haanen, M.S. Carlino, O. Bechter, M. Maio, I. Marquez-Rodas, M. Guidoboni, G. McArthur, C. Lebbe, P.A. Ascierto, G.V. Long, J. Cebon, J. Sosman, M.A. Postow, M.K. Callahan, D. Walker, L. Rollin, R. Bhore, F.S. Hodi, and J. Larkin. 2017. Overall Survival with Combined Nivolumab and Ipilimumab in Advanced Melanoma. *N Engl J Med*. 377:1345-1356.

Xue, W., L. Zender, C. Miething, R.A. Dickins, E. Hernando, V. Krizhanovsky, C. Cordon-Cardo, and S.W. Lowe. 2007. Senescence and tumour clearance is triggered by p53 restoration in murine liver carcinomas. *Nature*. 445:656-660.

Yang, M., and K.H. Vousden. 2016. Serine and one-carbon metabolism in cancer. *Nature reviews. Cancer*. 16:650-662.

Zhang, H., Z.H. Chen, and T.M. Savarese. 1996. Codeletion of the genes for p16INK4, methylthioadenosine phosphorylase, interferon-alpha1, interferon-beta1, and other 9p21 markers in human malignant cell lines. *Cancer Genet Cytogenet*. 86:22-28.

Zhao, R., B.Y. Choi, M.H. Lee, A.M. Bode, and Z. Dong. 2016. Implications of Genetic and Epigenetic Alterations of CDKN2A (p16(INK4a)) in Cancer. *EBioMedicine*. 8:30-39.

Zhu, X.G., A. Chudnovskiy, L. Baudrier, B. Prizer, Y. Liu, B.N. Ostendorf, N. Yamaguchi, A. Arab, B. Tavora, R. Timson, S. Heissel, E. de Stanchina, H. Molina, G.D. Victora, H. Goodarzi, and K. Birsoy. 2021. Functional Genomics In Vivo Reveal Metabolic Dependencies of Pancreatic Cancer Cells. *Cell metabolism*. 33:211-221.e216.